J14.5 MAINTAINING SNPP VIIRS REFLECTIVE SOLAR BAND SENSOR DATA RECORD QUALITY: ON-ORBIT UPDATE OF SCREEN TRANSMISSION AND SOLAR DIFFUSER BRDF PARAMERS

Evan Haas,* David Moyer, and Frank De Luccia
The Aerospace Corporation, El Segundo CA

1. INTRODUCTION

The Visible Infrared Imaging Radiometer Suite (VIIRS) on the Suomi National Polar Orbiting Partnership (SNPP) satellite collects radiometric and imagery data in 22 spectral bands within the visible and infrared region ranging from 0.4 to 12.5 μm. The satellite is polar-orbiting, sun-synchronous, with 14.2 orbits per day. VIIRS spectral data are calibrated and geolocated in ground processing to generate Sensor Data Records (SDRs). The VIIRS instrument has a rotating telescope assembly (RTA) that allows it to continuously collect data from the Earth view and several other calibration views. A full rotation of the VIIRS instrument is completed every 1.79 seconds, and a half-angle mirror (HAM) rotates at half the rate of the RTA to direct light into stationary optics and focal plane arrays.

Fourteen of the spectral bands are reflective solar bands (RSB) that are calibrated once per orbit by solar light passing through a solar attenuation screen (SAS) and reflected off of a solar diffuser (SD). An illustration of the VIIRS sensor with the SD and SDS is shown in figure 1. The ratio of the calculated to measured solar diffuser radiance is called the F factor and is trended during the mission. A more complete discussion of RSB calibration and the F factor can be found in Cardema (2012).

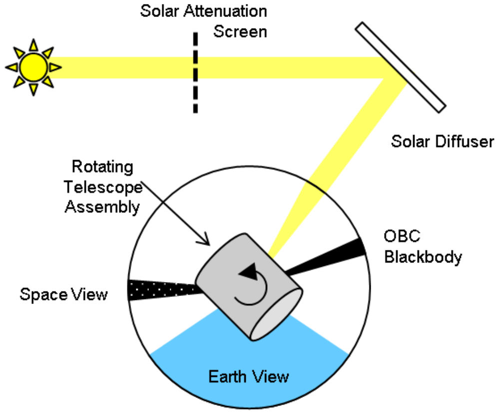

Figure 1. Illustration of the VIIRS RTA with associated views and solar calibration hardware.

The radiance when viewing the SD is a function of the SAS transmission and the SD's Bidirectional Reflectance Distribution Function (BRDF). The BRDF of the SD is expected to change throughout the mission, and the overall scale factor of this change is tracked and called the H factor. For a complete discussion of the H factor, see Haas (2012).

* Corresponding author address: Evan M. Haas, The Aerospace Corporation, P.O. Box 92957, M4/895, Los Angeles, CA 90009-2957; e-mail: Evan.M.Haas@aero.org

On-orbit changes in the H factor are monitored by a separate on-board instrument called the solar diffuser stability monitor (SDSM). It has been used during times of RSB calibration data collection at various frequencies throughout the mission (once per orbit to start, then reduced to once per day, and now 3 times per week). During a VIIRS scan, when the SDSM is operational, the SDSM collects 5 samples in one of 3 views: solar, SD, and dark reference. The SDSM is illustrated in figure 2. During a solar view, an attenuation screen called the SDSM screen reduces incoming solar radiance to levels comparable to those seen by the VIIRS sensor itself. During an SD view, the SDSM views the SD and the radiance is a function of the SAS transmission and the BRDF of the SD.

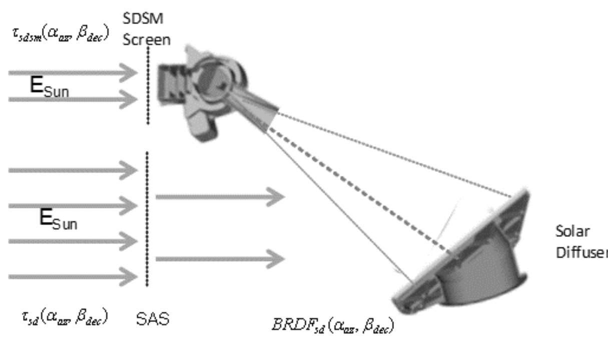

Figure 2. Illustration of the SDSM with solar and SD views.

Now, we will develop the equations for both the H and F factors. For the H factor, first we define the gain of an SDSM detector when viewing the SD, given by equation 1:

$$G_{sd} = \frac{DC_{sd} - DC_{bkg}}{E_{Sun} \cdot \tau_{sd}(\alpha_{az}, \beta_{dec}) \cdot \cos AOI_{sd} \cdot H \cdot BRDF(\alpha_{az}, \beta_{dec}) \cdot \sin^2(FOV_{sdsm})} \quad (1)$$

where DC_{sd}, and DC_{bkg} are the SDSM detector output counts from the SD and dark reference paths respectively, E_{sun} is the in-band solar irradiance at the satellite, $\tau_{sd}(\alpha_{az}, \beta_{dec})$ corresponds to the SAS transmittance as a function of solar azimuth α_{az} and declination β_{dec}, AOI_{sd} is the angle of incidence of sunlight on the SD, H is the BRDF degradation factor we seek to trend, $BRDF(\alpha_{az}, \beta_{dec})$ is the nominal BRDF as a function of solar angles, and FOV_{sdsm} is the half cone angle of the SDSM field of view. . Next, we define the gain of an SDSM detector when viewing the sun, given by equation 2:

$$G_{sun} \frac{DC_{sun} - DC_{bkg}}{E_{Sun} \cdot \tau_{ntn} \cdot \tau_{sdsm}(\alpha_{SDSMaz}, \beta_{SDSMel})} \quad (2)$$

where DC_{sun} is the SDSM detector output count from the Solar path, τ_{ntn} is the SDSM screen transmittance at normal incidence, and $\tau_{sdsm}(\alpha_{SDSMzz}, \beta_{SDSMdec})$ is the normalized SDSM screen transmittance, as a function of SDSM azimuth and SDSM elevation (transformed from solar azimuth and solar declination). Since the gains defined above are an intrinsic property of the SDSM and not a function of the source viewed, we can equate equations 2 and 3 and solve for the H factor, given in equation 3:

$$H = \frac{DC_{sd} - DC_{bkg}}{DC_{sun} - DC_{bkg}} \cdot \frac{\tau_{ntn} \cdot \tau_{sdsm}(\alpha_{az}, \beta_{dec})}{\tau_{sd}(\alpha_{az}, \beta_{dec}) \cdot \cos AOI_{sd} \cdot BRDF(\alpha_{az}, \beta_{dec}) \cdot sin^2(FOV_{sdsm})} \quad (3)$$

Now, as mentioned before, the F factor is a ratio of calculated to measured radiance of the VIIRS instrument, given in equation 4:

$$F = \frac{L_{calc}}{L_{meas}} = \frac{P_{sun} \cdot \tau_{sd}(\alpha_{az}, \beta_{dec}) \cdot \cos(AOI_{sd}) \cdot H \cdot BRDF(\alpha_{az}, \beta_{dec})}{4 \cdot \pi \cdot d_{se}^2 \cdot (\sum_{i=0}^{2} c_i(T_{det}, T_{elec}) \cdot dn^i)} \quad (4)$$

where L_{calc} is the calculated solar diffuser radiance, L_{meas} is the measured solar diffuser radiance, P_{sun} is the spectral solar power of the sun, $\tau_{sd}(\alpha_{az}, \beta_{dec})$ is the transmission of the solar diffuser screen, AOI_{sd} is the angle of incidence of sunlight on the solar diffuser, H is the H factor, $BRDF(\alpha_{az}, \beta_{dec})$ is the nominal BRDF as a function of solar angles, d_{se} is the earth-sun distance, dn is the offset corrected solar diffuser measured digital number, T_{det} is the detector temperature, T_{elec} is the electronics temperature, and c_i are temperature coefficients measured in pre-launch. The product of the spectrally dependent terms in the calculated radiance is averaged over wavelength using the relative spectral response, but this detail is omitted here for simplicity. The band, detector, gain state, and HAM side dependence of the F factor is also suppressed in equation (4) for simplicity.

The properties of the SDSM screen transmission along with the SD screen transmission and BRDF of the SD (from both the SDSM and RTA views) were characterized prelaunch and stored in look up tables (LUTs) that capture the variation of these parameters with solar geometry. It should be noted here that this paper addresses 3 LUTs: SDSM screen transmission, SD screen transmission times BRDF in the RTA view, and likewise in the SDSM view. The angular spacing of these LUTs was coarse and resulted in residuals which adversely affect H and in turn F factors. This paper addresses improvements to the SDSM screen transmission LUT and BRDF LUTs using on-orbit data, including a yaw maneuver that exposed VIIRS to a wide range of solar geometries in a short amount of time.

2. H FACTOR LOOK UP TABLE UPDATES

The H factor quantifies the gradual darkening of the SD. The H factor time series corresponding to all 8 SDSM detectors calculated using the operational LUTs are shown in figure 3. The detectors are in order of wavelength, with detector 1 being the shortest and also expected to have the greatest SD degradation. There are noticeable trend changes near orbit 11750 and 13200 which represent changes in SD radiance, further discussed in Haas (2015). Also, at various times throughout the mission, higher frequency modulations are apparent, such as large ones near orbit 11000. These higher frequency modulations do not reflect the expected characteristics of the SD degradation, but are rather attributed to screen transmission and BRDF LUT inaccuracies. The H factors shown in figure 3 were created with the current operational set of LUTs, which have been improved since launch. A similar process as the one being described here was applied after the yaw maneuver was performed. However, at that time there was a very limited set of mission history data to apply further refinements. The modulations that still exist in the operational H factors are a reflection of this fact.

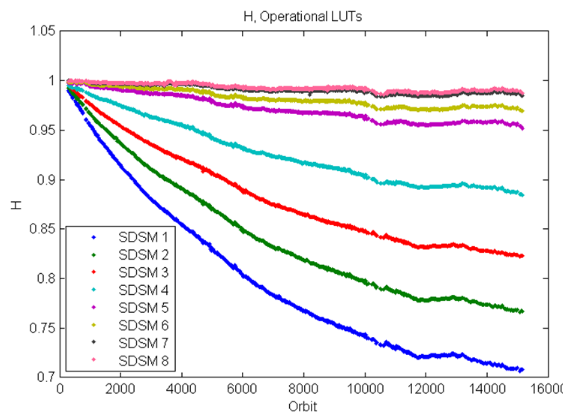

Figure 3. Current operational H factors versus orbit for all 8 SDSM detectors.

The degradation of the SD is expected to follow an exponential decay of some form. However, a variety of functional forms incorporating exponential decay have been found to provide nearly equivalent goodness of fit to the H factor time series. Extensive work has been performed to study these functional forms, and, as will be seen, care was taken to evaluate various forms for the purposes of these LUT improvements. For operationally delivered H factors, a 3 parameter fit is performed with the form A*exp(B*orbit)+C, where A, B, and C are the free parameters. A useful metric to quantify spurious modulations in the H factor is the “sum of RMS”, defined as the sum of the RMS values of the H fit residuals across all 8 SDSM detectors. Figure 4 shows the H fit residuals for operational H factors up to orbit 11700. The sum of RMS metric is included in the figure title. As improvements to the LUTs are developed in this paper, the sum of RMS metric can be used to compare the improvements relative to a baseline that uses existing operational LUTs.

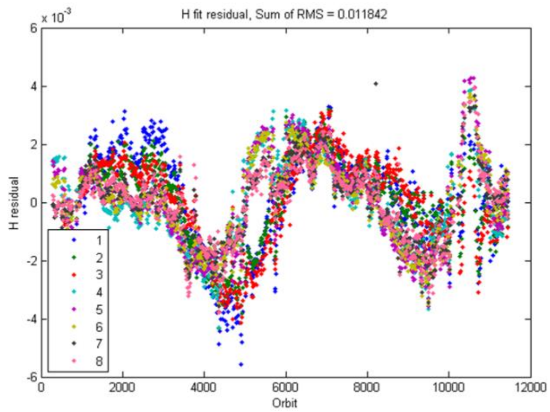

Figure 4. H fit residuals for all 8 SDSM detectors.

In order to re-derive SDSM screen transmission and SD BRDF LUTs, an understanding of VIIRS solar geometry is necessary. Figure 5 shows all relevant solar angles: solar declination, solar azimuth, SDSM elevation, and SDSM azimuth versus orbit. Solar and SDSM are related by a fixed rotation. A series of 14 yaw maneuvers were performed between orbits 1564 and 1578 to vary the solar and SDSM azimuths once per orbit, dwelling upon a fixed geometry during each time period when the sun illuminates the SD. The azimuth angles sampled during the maneuver are clearly evident in both the solar azimuth and SDSM azimuth plots. The fact that the yaw maneuver data were collected within one day is critical for re-derivation because the H factor was nearly constant while a large range of azimuths were sampled.

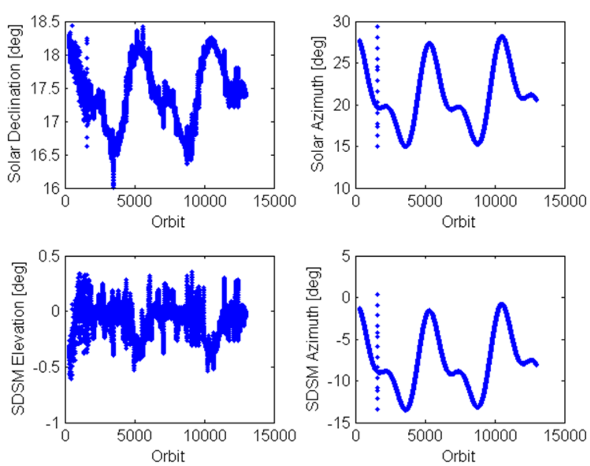

Figure 5. Solar and SDSM angles over the VIIRS mission history.

The first step in the LUT re-derivation process is to solve equation 2 for τ_{sdsm}. In order to actually calculate τ_{sdsm}, the solar gain values must be known. They are obtained from using a linear fit of solar gain values derived from current operational LUTs. The results of this calculation are plotted in a 3D plot in figure 6. The SDSM screen transmission values for SDSM detector 5 are plotted as a function of SDSM elevation and SDSM azimuth.

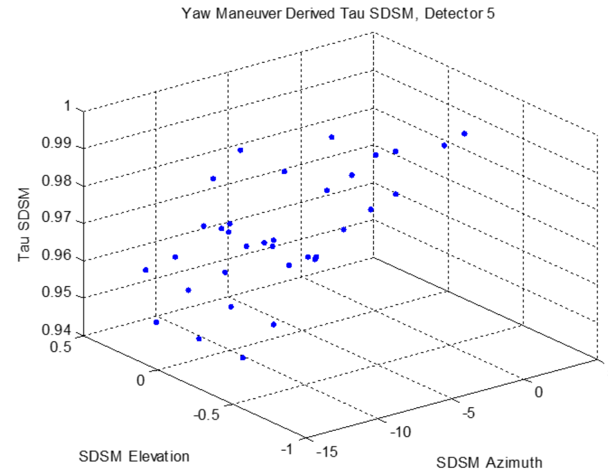

Figure 6. SDSM screen transmission as a function of SDSM elevation and azimuth for SDSM detector 5.

The next step in the process is to solve equation 3 for τ_{sd}*BRDF, the product of the SD screen transmission and BRDF in the SDSM view. Here, we must use a linear fit of H factors across the yaw maneuver time period, just as we did for solar gain in the previous step. Figure 7 shows τ_{sd}*BRDF as a function of solar declination and solar azimuth for SDSM detector 5.

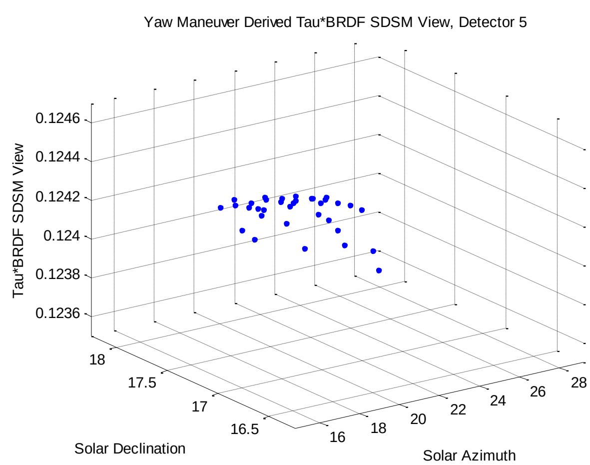

Figure 7. τ_{sd}*BRDF as a function of solar declination and solar azimuth for SDSM detector 5.

Once the 3 dimensional point clouds are created based on using yaw maneuver data, they must be interpolated and extrapolated to the solar geometry limits of the LUTs. Table 1 shows the solar geometry limits for both LUTs. In order to interpolate and extrapolate the point cloud, a thin plate spline was selected. The thin plate spline weighs both the smoothness of the fit and the residuals of the fit errors.

LUT	Min Vertical Angle	Max Vertical Angle	Min Horizontal Angle	Max Horizontal Angle
SD Screen Transmission	-2 deg SDSM Elevation	1.9 deg SDSM Elevation	-15 deg SDSM Azimuth	1.7875 deg SDSM Azimuth
τ_{sd}*BRDF, SDSM View	12.1083 deg Solar Declination	18.5 deg Solar Declinaion	13.5 deg Solar Azimuth	30.7813 deg Solar Azimuth
τ_{sd}*BRDF, VIIRS RTA View	12.0 deg Solar Declination	18.3917 deg Solar Declinaion	13.5 deg Solar Azimuth	30.7813 deg Solar Azimuth

Table 1. Solar Geometry limits for LUTs.

The results of applying the thin plate spline fit to the SDSM screen transmission data are shown in figure 8. The results for applying the thin plate spline fit to the τ_{sd}*BRDF data are in figure 9.

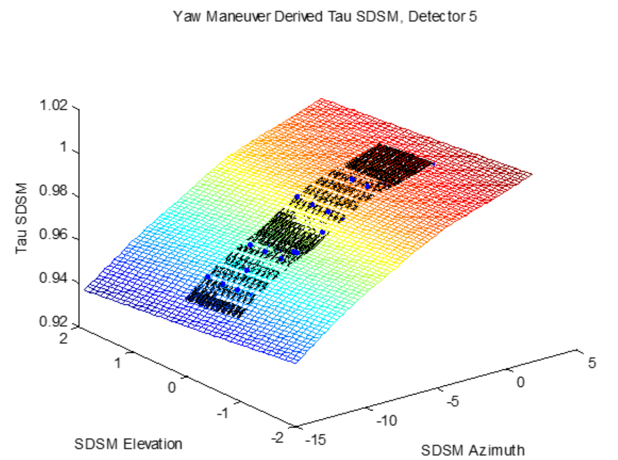

Figure 8. Thin plate spline fit of SDSM screen transmission data. Legend: blue dots are calculated points, black shading is interpolated region, and rainbow shading is extrapolated region.

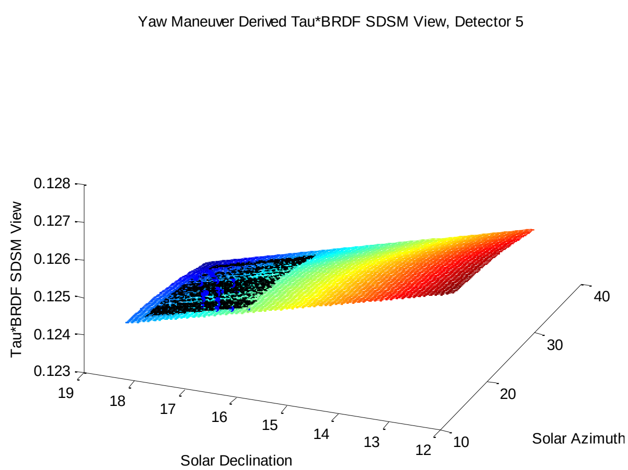

Figure 9. Thin plate spline fit of τ_{sd}*BRDF data. Legend: blue dots are calculated points, black shading is interpolated region, and rainbow shading is extrapolated region.

At this point in the process, the τ_{sd}*BRDF LUT is determined, however the SDSM transmission table will receive further enhancements. The next step in the process is to re-calculate H factors using the two new tables. Now, the H factor will be expected to have much larger modulations re-introduced, because these simple yaw maneuver derived tables have no corrections applied. The new H factor with these new LUTs is shown in figure 10. Residuals of the H factor fit up to orbit 11700 with sum of RMS metric are shown in figure 11. There is a threefold increase in sum of RMS, which matches our expectation that modulations will be reintroduced to the H factor.

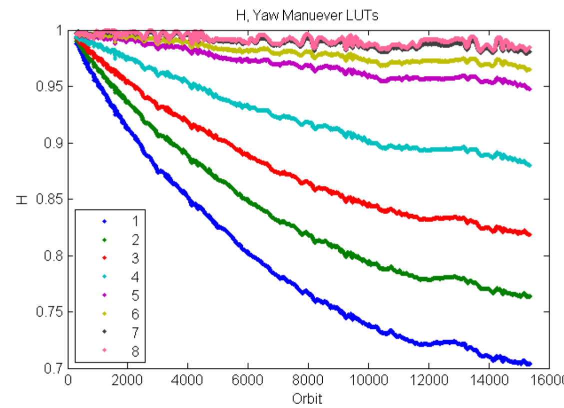

Figure 10. H factors after using the yaw maneuver defined LUTs.

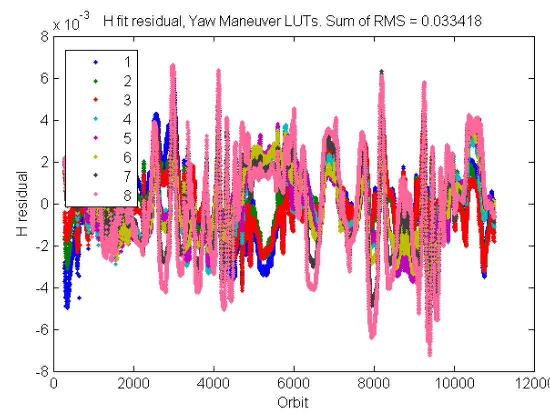

Figure 11. H fit residuals with yaw maneuver tables.

Now, corrections can be applied to the SDSM screen transmission table. First, the residuals in figure 11 are plotted against SDSM azimuth and elevation instead of orbit. Figure 12 shows residuals versus azimuth and figure 13 shows residuals versus elevation. There is clearly structure to the residuals shown versus SDSM azimuth, with peaking of residuals spaced in about two degree increments. Elevation, on the other hand, does not show such a clear pattern, and residuals look essentially uniformly distributed across angle. Several methods of applying corrections were evaluated, and the chosen method was to take the mean of the azimuth residuals in each angular bin of the LUT and add them to the transmission value. Table 1 shows the angular extents of the SDSM screen transmission LUT, and there are 80 azimuth angles stored in the LUT, meaning each angular bin spans 0.2098 deg. The value added at a given azimuth is added for all elevations, meaning this method does not account for changes in residual by elevation. One reason for this is that the residuals in each elevation bin average to essentially zero, meaning the correction is very small. One would think that the residuals could be averaged in 2 dimensions, across both SDSM azimuth and elevation, however this results in an under sampled space because there are not unique azimuth and elevation pairs to span the whole LUT.

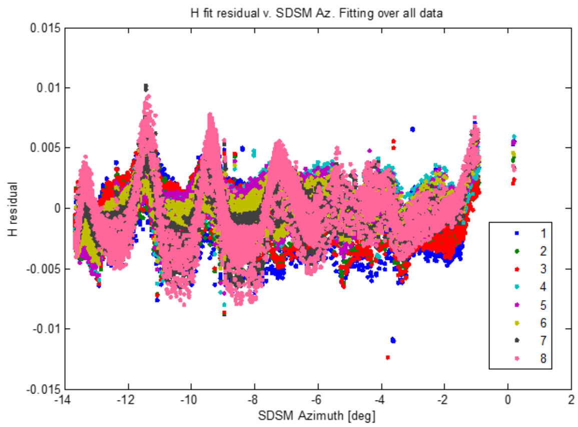

Figure 12. H fit residuals versus SDSM azimuth.

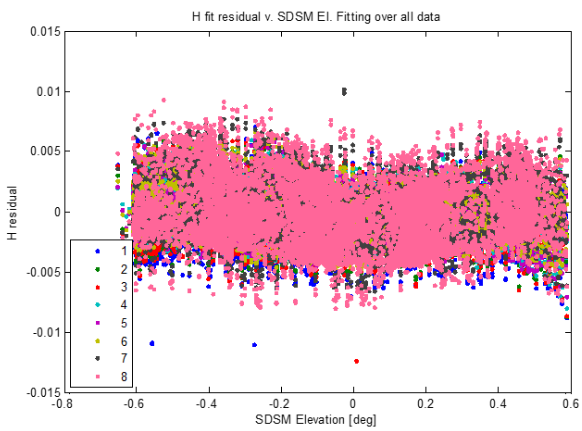

Figure 13. H fit residuals versus SDSM elevation.

The resulting SDSM transmission LUT is shown in figure 14 for SDSM detector 5. The overall shape of the table is relatively unchanged from the LUT in figure 8, but small features can be seen varying across SDSM azimuth and held constant in SDSM elevation. This is the same method as was applied in the current operational LUT, however the operational LUT had less than a year training period to generate corrections, and we are now using a two year training period.

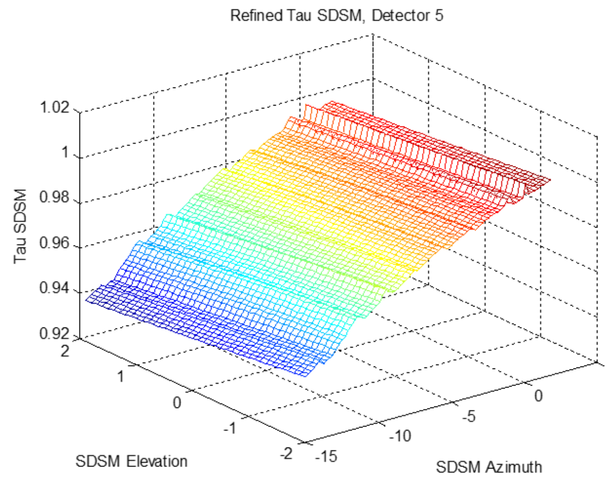

Figure 14. Azimuth corrected SDSM transmission LUT shown for SDSM detector 5.

With the corrected SDSM transmission LUT, H factors can again be generated. The new H factors are shown in figure 15 and the fit residuals are seen in figure 16. Now, the sum of RMS metric is less than half the starting value seen in figure 4. The H factors are also more visibly smooth, which corroborates the utility of the sum of RMS metric. Modulations after the training period (up to orbit 11700) are also smoothed, implying the method is robust outside of the training period.

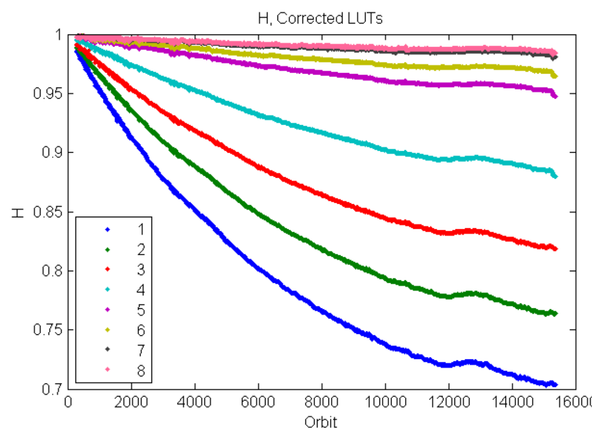

Figure 15. H factors with corrected LUTs.

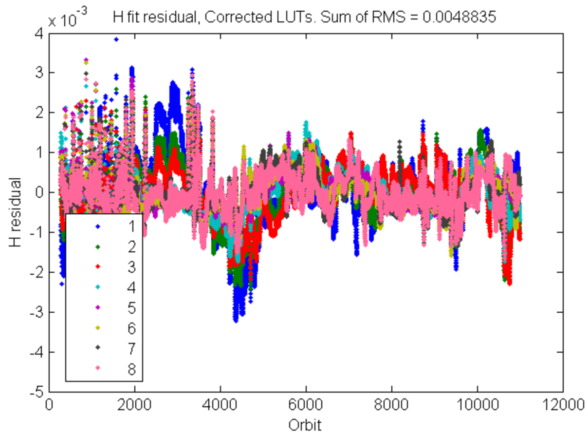

Figure 16. H fit residuals for corrected LUTs.

Several studies were performed to test the robustness of the overall LUT generation method. The first study was to investigate how the chosen training period influenced the results. In the applied method, the first two years were used as the training period, however these results were compared to using either the first year or second year alone. Table 2 compares the sum of RMS metrics for these 3 time periods, normalized to the chosen method of using two years. Using either the first year or second year results in over 20% poorer performance, and both results are very similar.

Training Period	Sum of RMS Normalized to Two Years
Two Years	1.000
First Year	1.224
Second Year	1.259

Table 2. Comparison of training periods with respect to normalized sum of RMS.

The second study was to evaluate the influence on results of the form of the function used to fit the H factor time series. Historical operational LUT updates used A*exp(B*orbit)+C as stated previously, so it was selected as the first form. However, there is no physical reason why this form should be chosen over others, so several more were evaluated. Table 3 shows the comparison of fitting forms with associated sum of RMS residuals normalized to the chosen (and historical) method. All three forms compared were less than 2% apart with respect to sum of RMS, and the improvement in the second fitting form was less than 1%. This means that the overall LUT improvement is essentially insensitive to the functional form chosen. Based on these results, use of the heritage functional form was selected for consistency with current operations.

Fit Functional Form	Sum of RMS Normalized to A*exp(B*orbit)+C
A*exp(B*orbit)+C	1.000
A*exp(B*orbit^2+C*orbit)	0.994
A*exp(B*orbit)+C*exp(D*orbit)	1.017

Table 3. Comparison of fit functional form with respect to normalized sum of RMS.

The third study was to iterate the LUT generation method, where each step begins with the prior set of LUTs and H factors. So, the H factors from figure 15 were the basis for generating new yaw maneuver tables as well as an updated SDSM transmission table. This objective of this study was to assess the stability of the LUT update method, as well as to possibly further refine the LUTs. Table 4 shows the final sum of RMS residuals for the two year training period after each iteration, normalized to the baseline set of LUTs. The 1st iteration shows over 3% improvement from the baseline run, and each subsequent iteration shows a slight improvement. The difference between the 2nd and 3rd iteration is only 0.1%, which shows the LUT update method is stable. Since the 3rd iteration produced the best sum of RMS number, the corresponding LUTs have been recommended for operational calibration.

Iteration Number	Sum of RMS Normalized to Baseline
Baseline	1.000
1	0.969
2	0.965
3	0.964

Table 4. Comparison of iterations with respect to normalized sum of RMS.

At this stage of the process, the H factor LUT improvements are considered complete. New SDSM transmission and τ_{sd}*BRDF LUTs were re-derived using yaw maneuver data. Unphysical modulations in the H factors were effectively removed by correcting the SDSM transmission LUT in azimuth space. The LUT improvements were shown to be robust to the choice of training period and to the choice of the functional form of the fitting function. The LUT improvements were also shown to be stable with respect to iteration of the improvement method after the second iteration, with virtually negligible improvement from the 2nd to the 3rd iteration. Now that H factors have been significantly improved via improved LUTs that reduce unphysical artifacts, F factors can be addressed with these new H factors as inputs.

3. F FACTOR LOOK UP TABLE UPDATE

The F factor in equation 4 has a dependence on the quantity τ_{sd}*BRDF just as the H factor did, although this quantity is now based on the SD viewing geometry of the VIIRS RTA rather than that of the SDSM. In order to create a new τ_{sd}*BRDF LUT based on yaw maneuver data, first F factors must be generated using new H factors. Then, equation 4 can be solved for τ_{sd}*BRDF just as was done with the H factor. Again, we use a linear fit for F factor values during the yaw maneuver for evaluation of τ_{sd}*BRDF. Then, a thin plate spline can be used again to interpolate and extrapolate over the extent of the LUT. Figure 17 shows the solved for τ_{sd}*BRDF values for the M1 band, HAM A, high gain, along with interpolation and extrapolation to LUT limits. Although the F factor has dependence on HAM side, gain state, and detector number, the τ_{sd}*BRDF LUT does not. To account for this, LUTs are made for every combination of HAM, gain, and detector for a given band and then averaged together.

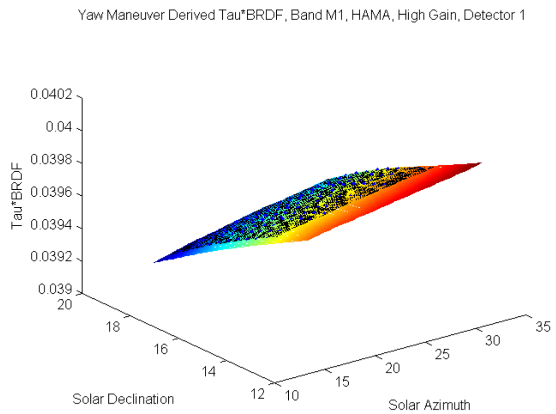

Figure 17. τ_{sd}*BRDF values for the VIIRS M1 band, HAM A, high gain, detector 1. Legend: blue dots are calculated points, black shading is interpolated region, and rainbow shading is extrapolated region.

F factors are then generated with the new yaw maneuver derived τ_{sd}*BRDF LUT. Figure 18 shows a comparison between the original F factor and the new F factor with the proposed τ_{sd}*BRDF LUT for band M1, detector 1, HAM A, gain high. The new F factors are qualitatively similar to current operational ones, but can differ by more than 0.1%, representing improvements in RSB calibration by this magnitude. Such improvements are significant for the VIIRS derived environmental products most sensitive to RSB calibration, such as ocean color.

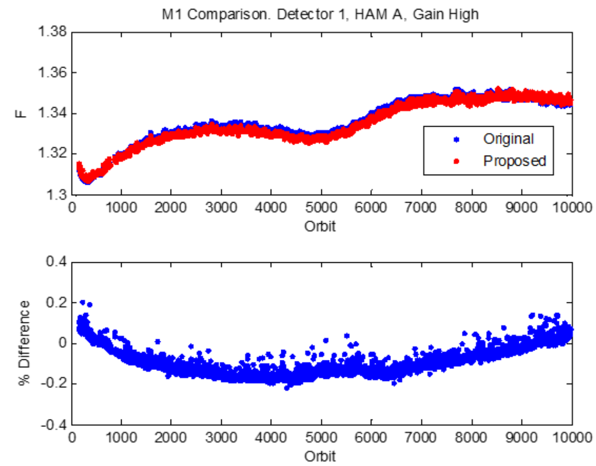

Figure 18. F factor comparison between original τ_{sd}*BRDF LUT and proposed. Band M1, HAM A, gain high, detector 1 shown. Also shown is a % difference plot comparing the two cases.

4. CONCLUSION

This paper discussed methods of improving SDSM screen transmission and τ_{sd}*BRDF LUTs. Improvements to these LUTs were demonstrated, which will in turn result in improvements to RSB calibration when the LUTs are implemented in operations. The two τ_{sd}*BRDF LUTs were created using yaw maneuver data, while the SDSM screen transmission LUT was also improved using data from the mission history. The transmission LUT was also demonstrated to be insensitive to the training period of mission history used, insensitive to the fitting form of the H factor time series, and stable to iterations of the LUT refinement process. New H factor LUTs resulted in a much smoother H factor time series that is believed to be more physical, based on an understanding of solar diffuser degradation. New F factors generated with new H factors and a new τ_{sd}*BRDF LUT in turn showed differences of more than 0.1%, which will result in an improvement in RSB calibration accuracy of the same magnitude.

5. REFERENCES

Cardema, J., Rausch, K. Lei, N., Moyer, D., De Luccia, F., 2012: Operational Calibration of VIIRS Reflective Solar Band Sensor Data Records, Proceedings of SPIE Vol. 8510, 851019

Haas, E., Moyer, D., De Luccia, F., et al., 2012: VIIRS solar diffuser bidirectional reflectance distribution function (BRDF) degradation factor operational trending and update, Proceedings of SPIE Vol. 8510, 851016

Haas, E., De Luccia, F., 2015: SNPP VIIRS Solar Diffuser BRDF Degradation Trend Changes in Early 2014, Poster presented at AMS 2015, Phoenix, Az.